Vikingsson, L.; Antolinos Turpín, CM.; Gómez-Tejedor, JA.; Ferrer Gallego, G.; Gómez Ribelles, JL. (2016). Prediction of the in vivo mechanical behavior of biointegrable acrylic macroporous scaffolds. Materials Science and Engineering: C. 61:651-658. doi:10.1016/j.msec.2015.12.068.

Materials Science & Engineering C (2016), pp. 651-658 doi: 10.1016/j.msec.2015.12.068

Prediction of the "*in vivo*" mechanical behavior of biointegrable acrylic macroporous scaffolds

L. Vikingsson[1,*], C. M. Antolinos-Turpin[1], J.A. Gómez-Tejedor[1], G. Gallego Ferrer[1,2], J.L. Gómez Ribelles[1,2]

[1]Centre for Biomaterials and Tissue Engineering (CBIT), Universitat Politècnica de València, Camino de Vera s/n, 46022 Valencia, Spain.
[2]Biomedical Research Networking Center in Bioengineering, Biomaterials and Nanomedicine (CIBER-BBN), Valencia, Spain.

*Corresponding author. Tel.: +34 963877007, ext.88939; fax: +34 963877276. E-mail: livi1@upv.es

Key words: Poly(Ethyl Acrylate) (PEA), Poly(2- Hydroxyl Ethyl Acrylate) (PHEA), Poly(Vinyl Alcohol), Freezing and thawing, Mechanical properties, Scaffold.

Abstract

This study examines a biocompatible scaffold series of random copolymer networks P(EA-HEA) made of Ethyl Acrylate, EA, and 2-Hydroxyl Ethyl Acrylate, HEA. The P(EA-HEA) scaffolds have been synthesized with varying crosslinking density and filled with a Poly(Vinyl Alcohol), PVA, to mimic the growing cartilaginous tissue during tissue repair. In cartilage regeneration the scaffold needs to have sufficient mechanical properties to sustain the compression in the joint and, at the same time, transmit mechanical signals to the cells for chondrogenic differentiation. Mechanical tests show that the elastic modulus increases with increasing crosslinking density of P(EA-HEA) scaffolds. The water plays an important role in the mechanical behaviour of the scaffold, but highly depends on the crosslinking density of the proper polymer. Furthermore, when the scaffold

with hydrogel is tested it can be seen that the modulus increases with increasing hydrogel density. Even so, the mechanical properties are inferior than those of the scaffolds with water filling the pores. The hydrogel inside the pores of the scaffolds facilitates the expulsion of water during compression and lowers the mechanical modulus of the scaffold. The P(EA-HEA) with PVA show to be a good artificial cartilage model with mechanical properties close to native articular cartilage.

1. Introduction

Tissue Engineering applies biology and engineering to regenerate damaged tissue and provide function to damaged organs[1]. Current tissue engineering techniques use three-dimensional porous scaffolds of natural or synthetic origin, sometimes previously seeded with cells. The scaffold material, pore architecture and cell source depend on the tissue application. Care is taken to develop materials that offer a suitable biomechanical environment, in such way that stress transmission to the cells hosted in the scaffolds pores is similar to surrounding tissue[2]. The cells inside the pores of the scaffold use mechanotransduction as one of the signalling paths to maintain their phenotype and produce the adequate extra-cellular matrix, ECM, components[3] [4] [5]. Accordingly, scaffold design is important since mechanical and physicochemical characteristics influence tissue response [6] [7]. Although cartilage is an anisotropic tissue, most papers than can be found in the literature for cartilage regeneration are based in isotropic 3D scaffolds and in some cases, some efforts have been done in the development of anisotropic materials for cartilage regeneration[8] [9] [10] [11] [12] [13] [14] [15]. Mechanical properties of the scaffold can be tailored by for example, modifying material, scaffold architecture or supplying chemical compounds. Articular cartilage is a tissue with relatively few cells embedded in a dense extra cellular matrix mainly composed of collagen type II and proteoglycans [16] [17] [18] [19] [20]. Chondrocytes receive and respond to mechanical stimuli by multiple regulatory

pathways that control extra cellular matrix production and function [21] [22] [23] [24] [25] [26] [27] [28]. Studies show that chondrocytes cultured under static conditions tend to loose chondrocytic phenotype and produce less extra cellular matrix components specific of articular cartilage, while dynamic culture under compression increases the amount of glycosaminoglycans produced of chondrocytes. The cellular effect depends on the applied load, the strain and frequency. [29] [30]

An important but often forgotten factor when designing and characterizing biomaterials is that the scaffold in a cartilage defect does not withstand the load in the joint by it self: *in vivo* pores are being filled with physiological liquid, cells and extra cellular matrix. In normal articular cartilage in humans tissue fluid represents between 65-85% of the total weight. Water is the most abundant component of articular cartilage. [31] Water and extra cellular matrix components contribute to the mechanical properties of the scaffold/cell construct and are time-depending, since the tissue is growing and get denser. Then, to comprehensively characterize a scaffold it is not sufficient to measure the mechanical modulus of the empty material, instead liquid immersed scaffold and ECM-like filled scaffold should be characterized. In a previous study we developed an experimental model to test the properties of macro and micro-porous scaffolds based on a Poly(Vinyl Alcohol), PVA, filling. This model was applied to predict the mechanical properties of Polycaprolactone, PCL, scaffolds implanted in articular cartilage defects [32]. The stiffness of the scaffold/hydrogel construct could be adjusted by different number of freezing and thawing (f/t) cycles and a mechanical response of the PCL/PVA construct close to native articular cartilage was obtained. PVA is a well studied polymer for tissue engineering applications and hydrogels produced by freezing and thawing, f/t, have interesting characteristics. By repeating cycles of f/t the aqueous solution of PVA crosslink by crystallite formation, and the crystallites increase in number with each cycle f/t [33] [34] [35] [36] [37] [38].

In this study we aim to use this experimental model to analyze the effect of crosslinking density on the mechanical response of macroporous acrylic polymers. Poly(Ethyl Acrylate), PEA, is a hydrophobic biocompatible polymer that has been tested for different tissue engineering applications. The cell response of PEA cultured supports has been favourable both in monolayer and in three dimensions, for human umbilical vein endothelial cells, conjunctival epithelial cells, fibroblasts, chondrocytes and osteoblasts [39] [39] [40] [41]. In particular it has been shown that PEA membranes are able to induce fibronectin fibrillogenesis in absence of cells, influencing cell adhesion, ECM organization and degradation, and cell differentiation [42] [43] [44]. In this study a series of scaffolds made of ethyl acrylate, EA, and hydroxyethyl acrylate, HEA, copolymers with weight proportion 90:10 have been prepared with varying amount of crosslinking agent Ethylene Glycol Dimethacrylate, EGDMA. By introducing a hydrophilic component favourable biological response can be obtained [8] [9]. The amount of crosslinking density is varied to be able to tailor the three dimensional structure and mechanical properties of the scaffold. PEA and P(EA-HEA) macro-porous scaffolds have been previously proposed for the anchoring ring of the cornea prosthesis [10]. In a recent study, a P(EA-HEA) scaffold has been used for cartilage regeneration in a rabbit model, showing that the scaffold guided cartilaginous tissue growth *in vivo* [45]. In this study, the P(EA-HEA) scaffold series has been filled with an aqueous solution of PVA and subjected to different cycles of freezing and thawing to tailor the mechanical properties. The role of the PVA hydrogel is to fill the P(EA-HEA) pores to simulate the ECM growing inside the pores, and in this way, to understand the mechanical response of the scaffold after implantation. In a future application of this materials for cartilage regeneration, the P(EA-HEA) will be implanted without the PVA. Unconfined compression test was made to evaluate the mechanical properties of empty and hydrogel filled scaffolds, while the scaffold morphology has been assessed by Scanning Electron Microscopy before and after mechanical assays.

2. Materials and Methods

2.1 Scaffold preparation

Scaffold series were prepared with a template technique previously reported elsewhere [46] [9] [47]. Templates were synthesized by use of Poly(Methyl Methacrylate), PMMA, microspheres (Colacryl DP 300, Lucite International, UK) with diameter between 80 and 120 μm. Porogen microspheres were placed in a metal mold and subjected to successive compressions at 150 ºC in a hot plates press (CUMIX TO-250/20). Templates were obtained in sheet form approximately 2 mm thick with a suitable interconnection of porogen particles. Mixtures of 90 % Ethyl Acrylate (99% Sigma-Aldrich, Spain), and 10% 2-Hydroxyethyl Acrylate (Sigma-Aldrich 96%, Spain), with 0.5 % Benzoine (98% Scharlau, Spain) and 1, 3 and 5% of crosslinking agent, Ethylene Glycol Dimethacrylate (99% Sigma-Aldrich, Spain) were prepared. The copolymers will be named P(EA-HEA) 1/3/5 to refer to each scaffold of the series. The monomer solutions were poured into transparent molds and radical polymerization took place for 24 hours under ultra violet radiation. A 24 hours post polymerization in 90ºC followed to ensure maximum monomer conversion. The sheets thus obtained were washed in acetone (99.9% Fluka, Spain) for 4 days at room temperature under stirring to eliminate the PMMA porogen microspheres. Acetone was changed three times. Porous three dimensional scaffolds were obtained by a slow acetone-water solvent exchange to extract the acetone and avoid pore collapse. Once obtained, water immersed scaffolds were left in water during 24 hours to assure no leftover traces of acetone. P(EA-HEA) membranes were cut into 3 mm diameter and 2 mm high scaffolds with circular stamps and surgical scalpels.

Porosity of both the porogen template and the P(EA-HEA) scaffolds (6 replica of each sample) was calculated using equation 1 where, m is the template weight of PMMA/scaffold, ρ is the polymer density and t, w and l are the height, width and length of the template, respectively [48].

$$\phi = 1 - \frac{m/\rho}{t \cdot w \cdot l} \quad (1)$$

Density of the PMMA template was determined through Archimedes principle. A Mettler AE 240 balance and Mettler ME 33360 accessory with sensitivity of 0.01 mg was used in measurements as described in others studies according to equation (2) [49] [50]. Dry samples were weighed in air (m_{air}) and in n-octane (m_{octane}) (95% Fluka, ρ=0.702 g/cm^3) three times per sample. Density was calculated as sample mass in air (m_{air}) divided by displaced volume of n-octane ($V_{displaced}$). The density value is 1.19 g/ for the PMMA spheres (supplier's value).

$$\rho = \frac{m_{air}}{V_{displaced}} \quad (2)$$

$$V_{displaced} = \frac{m_{air} - m_{octane}}{\rho_{octane}}$$

2.2 Hydrogel preparation

A 10% aqueous solution of PVA, average molecular weight, Mw, 130,000 Da and 99+% hydrolyzed (Sigma Aldrich, Spain) was prepared by continuously stirring at 90°C for 1 hour and then let cool down to room temperature. The solution was poured into with 5 mm diameter wells. Hydrogels were obtained by freezing the solution for 12 hours in -20°C and then thawed to room temperature for 8 hours in a chamber with saturated humidity. The f/t cycles was repeated for 1, 3 and 6 times.

The water content in the hydrogels after 6 f/t cycles was determined for six samples. Samples were freeze dried with -80°C and pressure < 100 mbar (Lyoquest, Telstar). The mass before and after freeze drying was measured and the difference was considered to be water. A Thermo Gravimetric Analysis (TGA/StarSystem, Mettler Toledo) to 400°C was done

to evaluate resting amount of water in the gel. The mass loss until 180°C was considered to be water.

The crystallinity in hydrogels after 1 and 6 number of f/t cycles was evaluated through Differential Scanning Calorimetry, DSC, analysis. As control an aqueous solution of PVA was cast to a Petri-dish and immediately frozen and freeze dried. DSC heating scans of the freeze dried gels and solution were performed at 20ºC/min in a PYRYS-DSC 8000 equipment (Perkin Elmer) under flowing nitrogen atmosphere between -80ºC and 280 ºC. The first scans revealed remaining water, especially for the low crosslinked hydrogels and a second scan was recorded. The samples were then heated to 100 ºC to remove the water contained by the samples and then a scan -80ºC and 280 ºC was done.

2.3 Scaffold/hydrogel construct

The PVA solution was introduced into the previously water-immersed P(EA-HEA) scaffolds by vacuum injection and the scaffold and gel constructs were frozen and thawed under the same conditions as the PVA gels. The effectiveness of the PVA filling was calculated with porosity calculations based on weight and dimensions of the samples according to equation 3. Porosity was calculated as volume of pores (V_{pores}) divided by total volume (V_{total}). The volume of pores was estimated as the difference in mass of scaffold with ($m_{with\ PVA}$) and without PVA solution (m_{dry}), divided by PVA solution density ($\rho_{PVA\ solution}$) The volume of the scaffold ($V_{scaffold}$) is calculated as the scaffold dry weight ($m_{dry)}$ divided by the polymer density ($\rho_{P(EA-HEA)}$). The density of the PVA solution was estimated from a 10% PVA aqueous solution with a pure PVA density of 1.30 g/cm^3 [51]. The density of P(EA-HEA) was calculated as described above.

$$\varnothing = \frac{V_{pores}}{V_{total}} = \frac{V_{pores}}{V_{scaffolds} - V_{pores}}$$

$$V_{pores} = \frac{m_{with\,PVA} - m_{dry}}{\rho_{PVA\,solution}} \quad (3)$$

$$V_{scaffold} = \frac{m_{dry}}{\rho_{P(EA-HEA)}}$$

2.4 Scanning Electron Microscopy

The morphology of the P(EA-HEA) scaffolds, the scaffold/gel construct and pure hydrogel was examined using a Scanning Electron Microscope SEM (JEOL JSM-5410, Japan) equipped with a cryogenic device. Samples were frozen at -90 °C, broken to see the cross-section of the samples and then sublimated during 40 minutes. The samples were gold sputtered and images were taken at an acceleration voltage of 10 kV.

2.5 Mechanical testing

The mechanical assays were performed using a Microtest SCM 3000 95 Universal Testing Machine (Spain) with a 15 N load cell at a strain rate of 1 mm/min. The samples were subjected to unconfined compression cycles to 15% strain at a rate of 1 mm/min, considering the physiological deformation of natural cartilage [52] [53] [54], in a custom-made device that allowed the samples to be immersed in water during the procedure. The results of this test were used to make a stress-strain representation and to calculate Young´s modulus at the slope of 2% deformation and the maximum stress at 15% deformation. [55]. The mechanical data was analyzed using ANOVA and where statistical difference was found an unpaired t-test was done. For each assay 6 samples of each group was tested. One way ANOVA can compare differences between more than two groups and the t-test is considered a special case of the one way ANOVA and can only compare two groups. The statistical differences are marked in the figures with asterisks to distinguish the groups.

3. Results and Discussion

3.1 Results

The porosity calculations for the porogen template and the P(EA-HEA) scaffolds are listed in table 1. The calculated density for P(EA-HEA) is 1.136 g/cm^3 . Porosities for scaffolds filled with PVA are all close to 0 and not shown. In table 1 it can be seen that the porosity is increasing slightly with increasing crosslinking density. The porosity of the PMMA template is 9 ± 5

which gives P(EA-HEA) scaffolds a theoretical porosity of 90%. The final porosity is slightly smaller, showing a certain contraction of the scaffold during template extraction. Materials with higher crosslinking density are closer to this value.

Material	ϕ (%)
P(EA-HEA) 1%	78 ± 4
P(EA-HEA) 3%	83 ± 3
P(EA-HEA) 5%	87 ± 4
PMMA template	9 ± 5

Table 1. The porosity of the porogen template and the P(EA-HEA) scaffolds without PVA hydrogel.

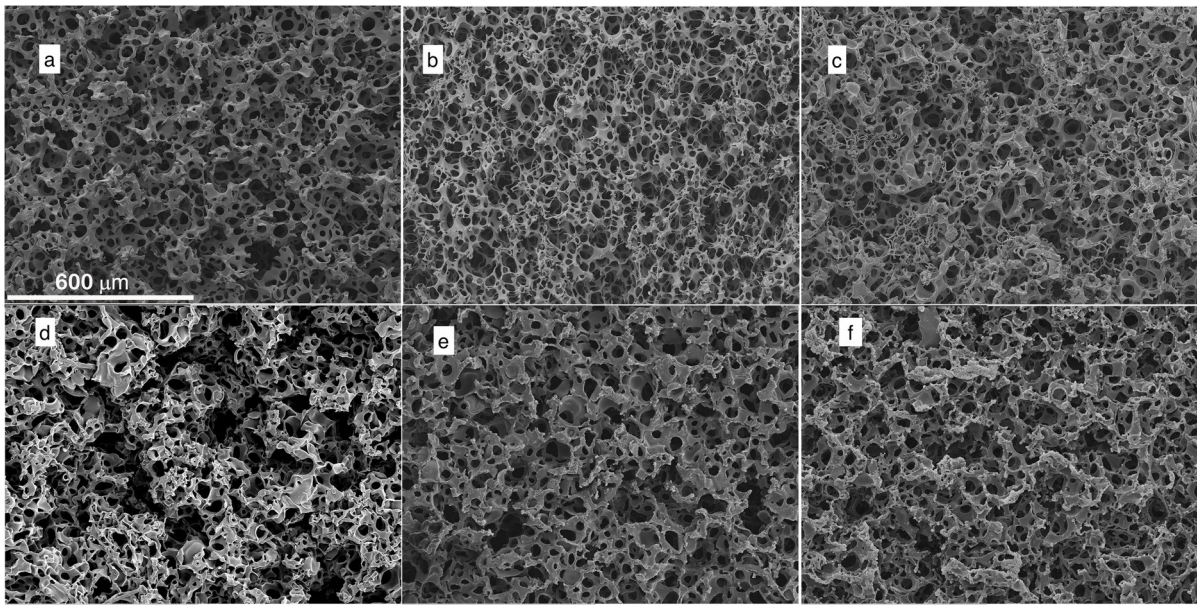

Figure 1. The morphology of the P(EA-HEA) 90:10 immersed scaffolds surface before (a-c) and after (d-f) compression tests: (a) and (d) 1% EGDMA, (b) and (e) 3% EGDMA and (c) and (f) 5 % EGDMA. Scale bar is valid for all pictures and corresponds to 600 μm

All the P(EA-HEA) scaffolds (Figure 1a-c) present an interconnected structure with spherical pores before compression tests. It is also possible to observe that the scaffold pores are more open and interconnected, with thinner trabeculare, for higher crosslinking density. The pore size was estimated from SEM images, taking 100 measuraments for each sample. The P(EA-HEA) 1% scaffolds show a pore size of 70±20 μm, the P(EA-HEA) 3% scaffolds 79±20 μm and the P(EA-HEA) 5% scaffolds 71±18 μm. The measured pore size between 70 and 80 μm is slightly smaller than the initial porogen size (between 80 and 120 μm) due to the contraction of the scaffold in the acetone-water solvent exchange. Figure 2 shows the histograms of the pore size distribution. We can observe that the distributions are right-skewed: the distribution is concentrated on the left of the figure, i.e., most of the pores are in the range of 50-80 μm for P(EA-HEA) 1% and 5% scaffolds, and in the range of 60-90 μm for P(EA-HEA) 3% scaffolds. Porosity values (Table 1) show that the porosity is increasing slightly with increasing crosslinking density. After compression tests all materials show a slight morphological change at the scaffold surface

(Figure 1 d-f), such as broken trabeculae. This effect is seen independently of the crosslinking density.

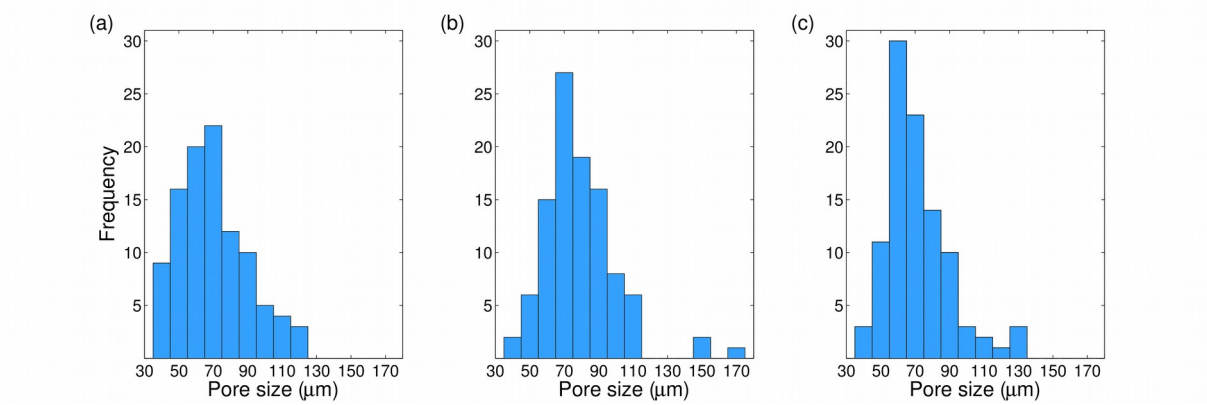

Figure 2. Pore size distribution for (a) the P(EA-HEA) 1% , (b) the P(EA-HEA) 3% and (c) the P(EA-HEA) 5% scaffolds.

The influence of crosslinking density on the mechanical properties of the porous scaffold has been assessed by comparing the scaffold with and without water in the pores. It is worth noticing that the P(EA-HEA) scaffold in this study is hydrophilic. The effect of water on the P(EA-HEA) scaffolds can only really be evaluated by testing the scaffolds without water in the macro-pores, but when the scaffold has absorbed water into the polymer. In this way, water in the macro-pores is the only difference between water-filled and water-absorbed samples. Consequently, the scaffolds were immersed in water, and then the water in the macro-pores were removed by absorption on filter paper. Both the modulus for the P(EA-HEA) scaffolds immersed in water and for the scaffolds with empty pores increases with increasing crosslinking density (Figure 3a-c). On the other hand, the scaffolds with empty pores (Figure 3a-c) show mechanical properties inferior to the water-immersed samples.

Another important observation is that the relationship between the elastic modulus of the water absorbed samples and the water filled samples for different crosslinking density differ. For increasing crosslinking density, 1%-3%-5% EGDMA, the modulus for the water absorbed samples is approximately: 0.05 - 0.1 - 0.3 MPa respectively. For the water immersed

samples the same scaffolds have modulus of approximately: 0.35 - 0.55 - 1 MPa. Consequently, the increase is not in the same order for the different samples. P(EA-HEA) 1% increase the modulus 7 times by having water in the pores, P(EA-HEA) 3% by 5 and P(EA-HEA) 5% increases the modulus 3 times.

a)

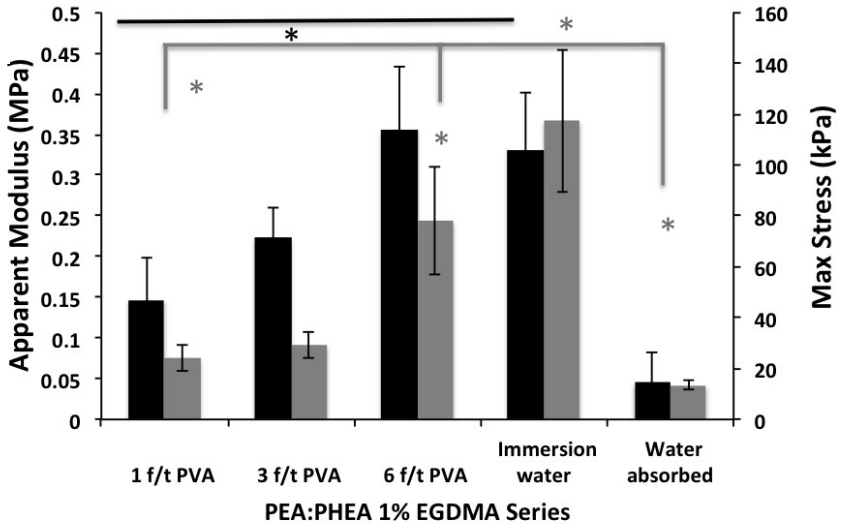

b)

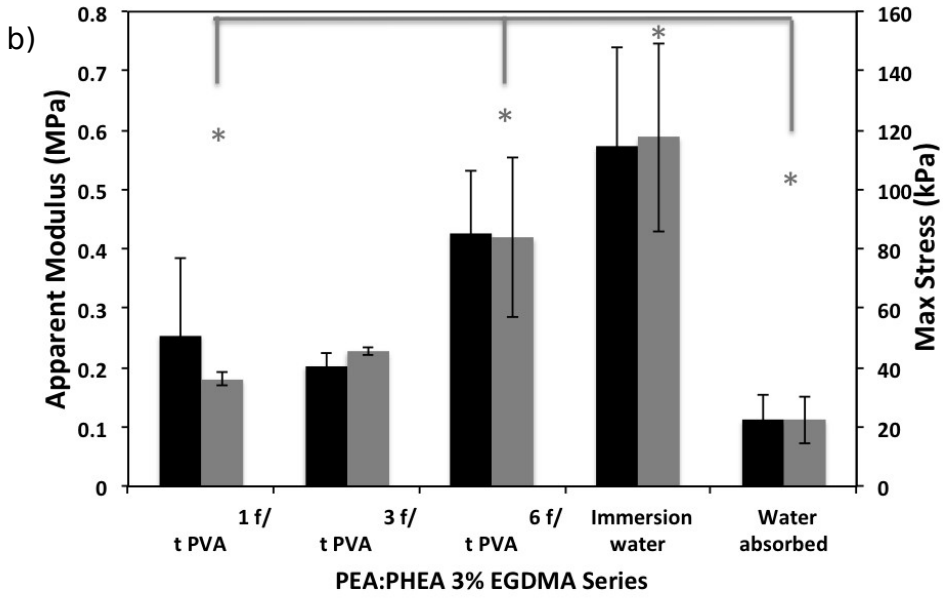

c)

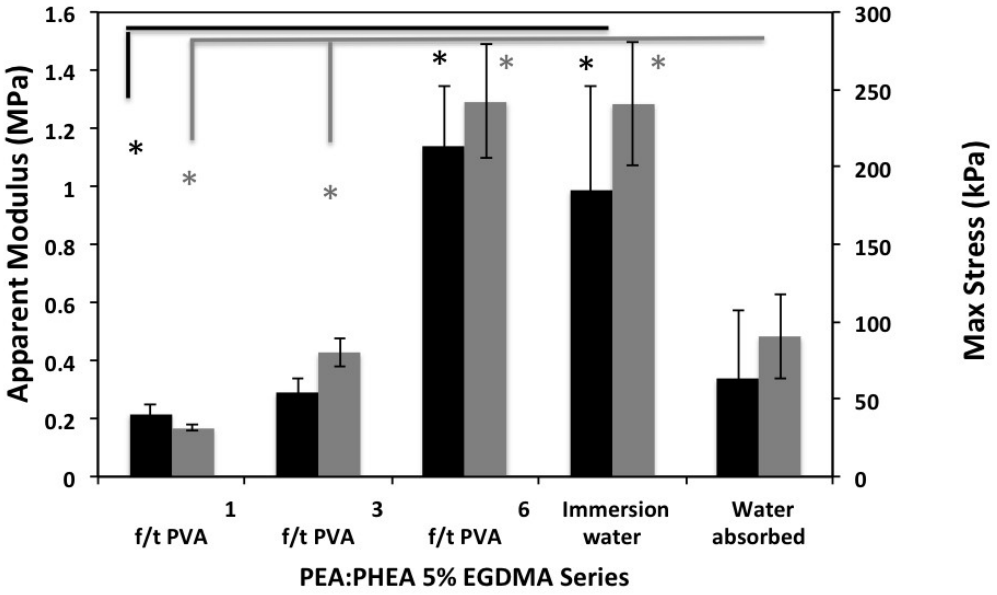

Figure 3. The elastic modulus (MPa) and stress for 15% strain in the unconfined compression tests for the P(EA-HEA) series, water absorbed, water immersed and filled with PVA hydrogel for 1, 3 and 6 cycles f/t: (a) P(EA-HEA) 1%, (b) P(EA-HEA) 3% and (c) P(EA-HEA) 5%. Black columns represent modulus (MPa) and grey stress for 15% strain (kPa). ANOVA statistical analysis and unpaired t-test (p< 0,05) were made between groups and significant difference is marked with an asterisk (black between modulus and grey between stress for 15% strain) in comparison with 1 cycle f/t.

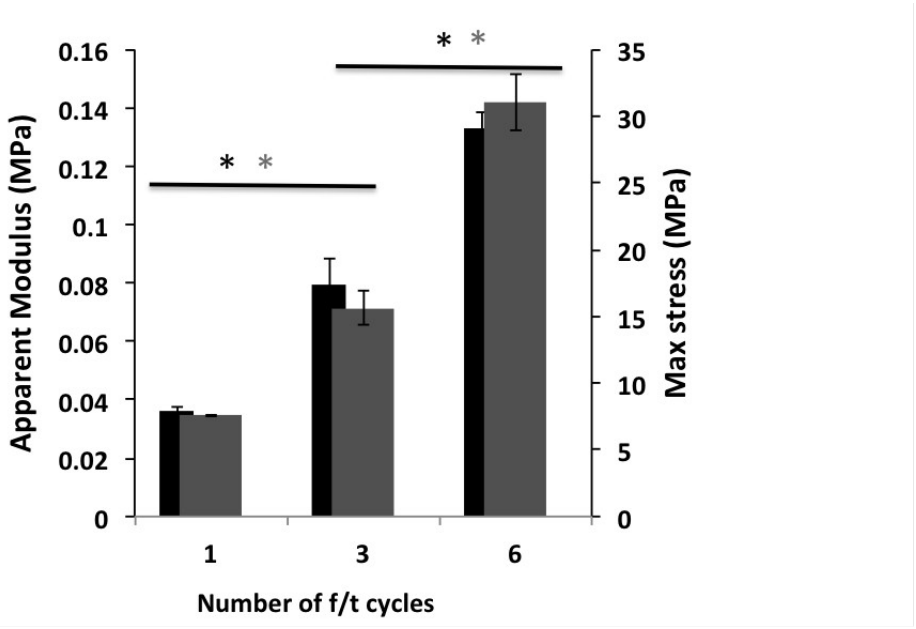

Figure 4. PVA gel subjected to 1, 3 and 6 cycles of freezing and thawing in unconfined compression tests in immersed conditions. Black columns represent modulus (MPa) and grey stress for 15% strain (kPa). ANOVA statistical analysis and unpaired t-test (p< 0,05) were made between groups and significant difference is marked with an asterisk (black between modulus and grey between stress for 15% strain) in comparison with 1 cycle f/t.

In figure 4 it can be seen that the mechanical properties of the pure PVA gels increase with the number of freezing and thawing cycles. The water content of the pure PVA hydrogels after 6 f/t cycles was measured as mass loss after freeze drying followed by TGA analysis. The water content after freeze drying was calculated to 86.7 %. TGA analysis show that the freeze dried samples still contained 4.1 % water. Hence, total amount of water in the initial samples were 87.2 %.

The crystallinity of the pure PVA gels after 0, 1 and 6 f/t cycles was calculated from DSC scans as melting enthalpy divided by ΔH_m^o for a pure crystalline PVA sample, 150 J/g [56]. Results are shown in table 2. The crystallinity varied from 46 % to 54 % from solution to 6 f/t cycles. This is

coherent with others results, that report crystallinity values of 56% in hydrogels after 10 cycle f/t [57].

Sample	Crystallinity (%)
PVA 0 cycles f/t	46.4
PVA 1 cycles f/t	48.6
PVA 6 cycles f/t	54.7

Table 2. The crystallinity of the PVA solution and hydrogels calculated from DSC scans.

When the PVA solution is introduced into P(EA-HEA) 1% scaffolds and subjected to 6 cycles of f/t (Figure 5a) it can be seen that the hydrogel enters all the scaffolds pores. SEM images of the cross-sektion of the scaffold/hydrogel construct after compression tests (Figure 5b) show a slighly different morphology, with a dense gel that seems affected by compression. SEM images of pure PVA hydrogel after 1, 3 and 6 cycles f/t show a porous structure with a disperse pore size (0.5-2 μm) for all cycles of f/t. Figure 5c shows the hydrogel after 6 cycles f/t, which is representative for all cycles f/t.

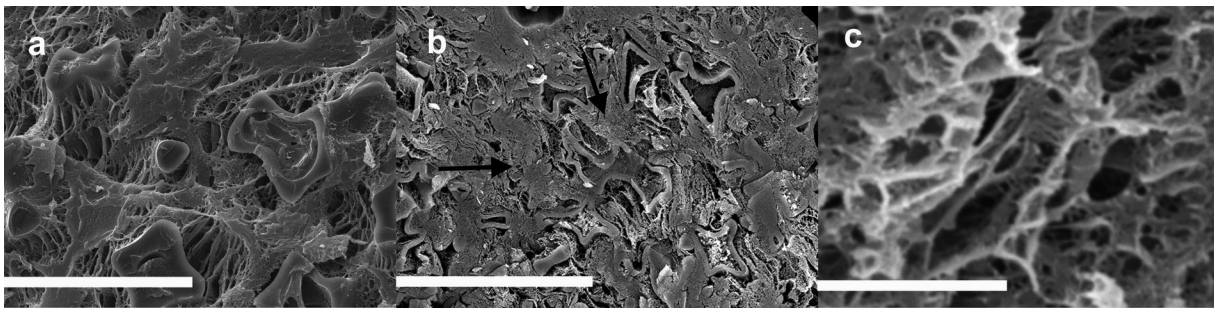

Figure 5. (a) The cryoSEM images of the cross-section of P(EA-HEA) 1% scaffold filled with PVA 6 cycles f/t. The scaffold is completely filled with hydrogel. Scale bar 80 μm. (b) The cryoSEM image of P(EA-HEA) 1% filled with PVA 6 cycles f/t after compression tests. The hydrogel is indicated with black arrows. Scale bar 80 μm. c) The crySEM image of the pure PVA hydrogel before compression tests, for 6 cycles of freezing and thawing. Scale bar 4 μm.

The mechanical modulus of the hydrogel-filled scaffolds increases for increasing number of freezing and thawing cycles. However, the modulus is lower than for the water-immersed scaffolds. When the hydrogel is densely crosslinked, after 6 cycles of freezing and thawing, the modulus reach the same value as for the water-immersed scaffold.

3.2 Discussion

For the P(EA-HEA) scaffolds with different crosslinking density it is seen a small pore size, and porosity increase with increasing crosslinking density (Table 1). This phenomenon is produced during the solvent exchange process from acetone to water in the scaffold synthesis. The material with higher crosslinking density absorb less acetone which maintains the material rigid during the the solvent exchange, and the result is an interconnected and open pore structure. The scaffolds with smaller crosslinking density can absorb greater amount of acetone and soften during the solvent exchange, which will close the pores.

When the scaffolds mechanical properties were evaluated in unconfined compression tests, in water immersed and water absorbed conditions interesting features could be seen. The scaffolds with empty pores (Figure 3a-c) show mechanical properties inferior to the water-immersed samples. This indicates that it is foremost water movement inside the scaffold pores that determines the mechanical properties of the scaffold.

Another interesting observation is made comparing the elastic modulus values of the water immersed and water absorbed samples for different crosslinking density. The different samples increase the modulus differently, depending on the crosslinking grade. P(EA-HEA) 1% increase the modulus 7 times, P(EA-HEA) 3% by 5 and P(EA-HEA) 5% increases the modulus 3 times. This means that the stiffness of the proper polymer network influence the effect of water on the mechanical properties. As the

polymer network becomes more crosslinked, and consequently stiffer, the effect of water filling is less important for the mechanical outcome. On the other hand, there is also a difference in porosity and pore-size between the samples. The decrease in porosity increases tortuosity of the water flowing through the scaffold during compression. This makes the water passage more difficult and hence, the compressive modulus increases.

Unmistakably, the capacity of reaching realistic conclusions about the *in vivo* behavior of the scaffolds is limited with these measurements. The scaffold, when implanted in a chondral defect, will be filled progressively by cells and ECM molecules that form a dense tissue. The PVA hydrogel inside the pores of the scaffold therefore gives a realistic simulation of the *in vivo* situation. By subjecting the scaffold/hydrogel construct to repeated number of freezing and thawing cycles the PVA becomes stiffer and can be compared to repair tissue. The PVA stiffness can be tailored from an almost viscous solution to a hard hydrogel, simulating the growing tissue inside the scaffold pores.

In this study the macro porous P(EA-HEA) scaffolds with different crosslinking density were filled with an aqueous solution of Poly(Vinyl Alcohol) and subjected to 1, 3 and 6 cycles of freezing and thawing. Porosity results and SEM images show that the PVA enters all pores in the scaffold. The mechanical properties of the pure PVA hydrogels increase with increasing number of f/t cycles (Figure 4), and the same pattern can be seen for the hydrogel filled scaffolds (Figure 3), albeit not always significant differences are found. In all P(EA-HEA) scaffolds filled with PVA the elastic modulus increases with respect to the pure PVA gel. Interestingly enough the mechanical properties for the PVA filled scaffolds decrease compared to the scaffolds immersed in water. When a soft hydrogel is inside the scaffold pores, the water flow is facilitated and expulsed more easily why also the mechanical properties decrease. Only for samples with 6 cycles of f/t the mechanical properties are as for the water immersed scaffolds.

The increase in elastic modulus in the water filled samples, in comparison to the empty scaffolds, is explained by the water expulsion through the scaffold. The decrease in elastic modulus in the hydrogel filled samples is also explained by the water flow through the sample. The presence of a soft gel inside the pores makes the water flow easier and thus, increases the compliance of the scaffold. It is worth to notice that the situation is quite different from that of a scaffold with both macro and micro-pores. In previous studies with a Polycaprolactone scaffold filled with PVA hydrogel [32] [58] [59], there was no difference in the elastic modulus for dry and water immersed scaffolds. The PCL scaffold is fabricated with a freeze extraction and particle leaching method [60] [61] [62] [63] [64] that generates both macro and micro-pores in the scaffold walls. The fact that the water immersed and dry PCL scaffold showed similar mechanical properties, whereas the macro-porous P(EA-HEA) scaffold showed a significant difference between the dry and water immersed samples reveals the role of micro-porosity on water flow and mechanical properties. In the case of the macro and micro-porous PCL scaffold, a relative high compression velocity makes the water expulsion from the pores fast and the modulus is similar for samples with and without water. The micro-porosity seems to increase the water expulsion and hence, lower the elastic modulus. Considering that the P(EA-HEA) only have macro-pores, water expulsion is not that fast and the elastic modulus increases. Once filled with a densely crosslinked hydrogel, the scenario is different, since all the pores are filled with hydrogel. The elastic modulus for the hydrophobic PCL increased significantly filled with PVA 6 f/t cycles, on the contrary the P(EA-HEA) scaffolds filled with PVA 6 f/t have the same modulus as the water immersed samples. This can be due to that hydrophilic P(EA-HEA) samples filled with hydrogel makes the water expulsion easier, compared to hydrophobic PCL scaffolds. On the other hand when the micro-pores are filled with densely crosslinked hydrogel, water expulsion is impeded and this double pore architecture can prevent water flow even more and increase the modulus.

These results are interesting since they indicate the performance of the scaffold once implanted in a chondral defect. Immediately after implantation, the scaffold pores would be filled with fluid and cells, a scenario similar to the water immersed scaffolds. When the tissue grow, the scaffold/tissue can be compared to the scaffold/hydrogel model for different cycles of f/t. Apparently, the initial modulus of the P(EA-HEA) scaffolds would be similar to the water immersed scaffolds. Then, it would decrease in the fist stages of tissue regeneration and with time increase, when the repair tissue inside the scaffold impede water flow through the porous structure.

Comparing the values of elastic modulus to articular cartilage in a rabbit model, 0.41 ± 0.12, MPa [65] and human, 0.581 ± 0.168 MPa [66], it can be seen that the P(EA-HEA) 1% reaches values of the rabbit model for immersed samples. P(EA-HEA) 1% filled with PVA 6 cycles f/t and P(EA-HEA) 3% and 5% immersed in water or filled with PVA 6 cycles f/t have values close to those of human articular cartilage.

4. Conclusions

This study evaluates the mechanical properties of P(EA-HEA) scaffolds made with a porogen template technique for different crosslinking density. The scaffolds have been tested empty, water immersed or filled with PVA hydrogel subjected to different number of freezing and thawing cycles. It can be seen that the P(EA-HEA) scaffolds have increasing porosity with increasing crosslinking density, due to the solvent exchange in the synthesis method. Furthermore it can be observed that the PVA hydrogel enters all the scaffold pores, confirmed by porosity measurements and SEM photos. The PVA hydrogels show increasing crystallinity and decreasing water content with increasing number of freezing and thawing cycles. The SEM images show that the compression test have not damaged or collapsed the scaffold pores. The elastic modulus increases with increasing crosslinking density for the P(EA-HEA) scaffolds. The results are interesting as they allow tailoring P(EA-HEA) scaffolds with different

amount of crosslinking agent. When excess water is removed and the scaffolds are tested in dry conditions the modulus decreases, which show the effect of water inside the scaffold pores. When the scaffolds are filled with a soft hydrogel, the elastic modulus is in the same range as for the dried samples. The soft hydrogel facilitates water flow out of the scaffold during compression and the modulus decreases. When the hydrogel is more crosslinked, the modulus increases but only to values of water immersed scaffolds. This indicates that the water flow inside the scaffold pores is a key factor for determining mechanical properties. The results from hydrogel filled samples give a realistic approximation of the *in vivo* behavior of the scaffolds. PVA is a good cartilage model simulating ECM growth inside the scaffolds pores. The mechanical modulus for the P(EA-HEA)/PVA constructs is similar as for native articular cartilage.

Acknowledgements:

This work was funded by the Spanish Ministry of Economy and Competitiveness (MINECO) through the project MAT2013-46467-C4-1-R (including the FEDER financial support). CIBER-BBN is an initiative funded by the VI National R&D&i Plan 2008–2011, Iniciativa Ingenio 2010, Consolider Program. CIBER actions are financed by the Instituto de Salud Carlos III with assistance from the European Regional Development Fund. The authors acknowledge the assistance and advice of Electron Microscopy Service of the UPV.

References

1. Langer, R. & Vacanti, J. P. Tissue engineering. *Science (80-.).* **260,** 920–926 (1993).

2. Hutmacher, D. W. Scaffold design and fabrication technologies for engineering tissues - state of the art and future perspectives. *J Biomater Sci-Polym Ed* **12,** 107–124 (2001).

3. Chiquet, M., Renedo, A. S., Huber, F. & Flück, M. How do fibroblasts translate mechanical signals into changes in extracellular matrix production? *Matrix Biol* **22,** 73–80 (2003).

4. Ingber, D. E. Tensegrity: the architectural basis of cellular mechanotransduction. *Annu. Rev. Physiol* **59,** 575–599 (1997).

5. Gelles, J. Transcription against an applied force. *Science (80-.).* **270,** 1650–1657 (1995).

6. Hutmacher, D. W. Scaffolds in tissue engineering bone and cartilage. *Biomaterials* **21,** 2529–2543 (2000).

7. Hendriks, J. A., Moroni, L., Riesle, J., de Wijn, J. R. & van Blitterswijk, C. A. The effect of scaffold-cell entrapment capacity and physico-chemical properties on cartilage regeneration. *Biomaterials* **34,** 4259–4265 (2013).

8. Escobar, JL, et al. Proliferation and differentiation of goat bone marrow stromal cells in 3D scaffolds with tunable hydrophilicity. *J. Biomed. Mater. Res. B. Appl. Biomater.* **91,** 277–86 (2009).

9. Diego, R. B. *et al.* Acrylic scaffolds with interconnected spherical pores and controlled hydrophilicity for tissue engineering. *J Mater Sci Mater Med.* **16,** 693–698 (2005).

10. Alio del Barrio, J. L. *et al.* Biointegration of corneal macroporous membranes based on poly(ethyl acrylate)

copolymers in an experimental animal model. *J. Biomed. Mater. Res. A* **103,** 1106–1118 (2015).

11. Kim, S. H., Kim, S. H. & Jung, Y. TGF-beta3 encapsulated PLCL scaffold by a supercritical CO2-HFIP co-solvent system for cartilage tissue engineering. *J. Control. Release* **206,** 101–107 (2015).

12. Yin, F. *et al.* Cartilage Regeneration of Adipose-Derived Stem Cells in the TGF-beta1-Immobilized PLGA-Gelatin Scaffold. *Stem Cell Rev.* **11,** 453–459 (2015).

13. Gruchenberg, K. *et al.* In vivo performance of a novel silk fibroin scaffold for partial meniscal replacement in a sheep model. *Knee Surg. Sports Traumatol. Arthrosc.* **23,** 2218–2229 (2015).

14. Arora, A., Kothari, A. & Katti, D. S. Pore orientation mediated control of mechanical behavior of scaffolds and its application in cartilage-mimetic scaffold design. *J. Mech. Behav. Biomed. Mater.* **51,** 169–183 (2015).

15. De Mulder, E. L. W., Hannink, G., van Kuppevelt, T. H., Daamen, W. F. & Buma, P. Similar hyaline-like cartilage repair of osteochondral defects in rabbits using isotropic and anisotropic collagen scaffolds. *Tissue Eng. Part A* **20,** 635–645 (2014).

16. Eyre, D. Collagen of articular cartilage. *Arthritis Res.* **4,** 30–35 (2002).

17. Roughley, P. J. & Lee, E. R. Cartilage proteoglycans: structure and potential functions. *Microsc Res Tech* **28,** 385–397 (1994).

18. Newman, A. P. Articular Cartilage Repair. *Am. J. Sport. Med.* **26,** 309–324 (1998).

19. Cameron, D. A. & Robinson, R. A. Electron Microscopy of Epiphyseal and Articular Cartilage Matrix in the Femur of the Newborn Infant. *J. Bone & Jt. Surg.* **40,** 163–170 (1958).

20. Eichelberger, L., Roma, M. & Moulder, P. V. Biochemical Studies of Articular Cartilage. *J. Bone & Jt. Surg.* **41,** 1127–1142 (1959).

21. Sims, J. R., Karp, S. & Ingber, D. E. Altering the cellular mechanical force balance results in integrated changes in cell, cytoskeletal and nuclear shape. *J. Cell Sci.* **103,** 1215–1222 (1992).

22. Enomoto, M., Leboy, P. S., Menko, A. S. & Boettiger, D. β1 Integrins Mediate Chondrocyte Interaction with Type I Collagen, Type II Collagen, and Fibronectin. *Exp. Cell Res.* **205,** 276–285 (1993).

23. Adams, J. C. & Watt, F. M. Regulation of development and differentiation by the extracellular matrix. *Development* **117,** 1183–1198 (1993).

24. Valhmu, W. B. *et al.* Load-controlled compression of articular cartilage induces a transient stimulation of aggrecan gene expression. *Arch. Biochem. Biophys.* **353,** 29–36 (1998).

25. Elder, B. D. & Athanasiou, K. A. Hydrostatic pressure in articular cartilage tissue engineering: from chondrocytes to tissue regeneration. *Tissue Eng Part B Rev.* **15,** 43–53 (2009).

26. Takahashi, K. *et al.* Hydrostatic pressure influences mRNA expression of transforming growth factor-beta 1 and heat shock protein 70 in chondrocyte-like cell line. *J. Orthop. Res.* **15,** 150–158 (1997).

27. Ragan, P. M. *et al.* Down-regulation of chondrocyte aggrecan and type-II Collagen gene expression correlates with increases in static compression magnitude and duration. *J. Orthop. Res.* **17,** 836–842 (1999).

28. Sah, R. L., Grodzinsky, A. J., Plaas, A. H. & Sandy, J. D. Effects of tissue compression on the hyaluronate-binding properties of newly synthesized proteoglycans in cartilage explants. *Biochem. J.* **267,** 803–808 (1990).

29. Bryant, S., Chowdhury, T., Lee, D., Bader, D. & Anseth, K. Crosslinking density influences chondrocyte metabolism in dynamically loaded photocrosslinked poly(ethylene glycol) hydrogels. *Ann Biomed Eng .* **32,** (2004).

30. Appelman, T., Mizrahi, J., Elisseeff, J. & Seliktar, D. The influence of biological motifs and dynamic mechanical stimulation in hydrogel scaffold systems on the phenotype of chondrocytes. *Biomaterials* **32,** 1508–1516 (2011).

31. Mow, V. C., Ratcliffe, A. & Poole, A. R. Cartilage and diarthrodial joints as paradigms for hierarchical materials and structures. *Biomaterials* **13,** 67–97 (1992).

32. Vikingsson, L., Gallego Ferrer, G., Gómez-Tejedor, J. A. & Gómez Ribelles, J. L. An in vitro experimental model to predict the mechanical behaviour of macroporous scaffolds implanted in articular cartilage. *J. Mech. Behav. Biomed. Mater.* **32,** 125–31 (2014).

33. Stasko, J., Kalniņš, M., Dzene, A. & Tupureina, V. Poly(vinyl alcohol) hydrogels. *Proc. Est. Acad. Sci.* **58,** 63–66 (2009).

34. Grant, C. *et al.* Poly(vinyl alcohol) Hydrogel as a Biocompatible Viscoelastic Mimetic for Articular Cartilage. *Biotechnol. Prog.* **22,** 1400–1406 (2006).

35. Spiller, K. L., Laurencin, S. J., Charlton, D., Maher, S. A. & Lowman, A. M. Superporous hydrogels for cartilage repair: Evaluation of the morphological and mechanical properties. *Acta Biomater.* **4,** 17–25 (2008).

36. Hassan, C. M. & Peppas, N. A. in *Biopolymers · PVA Hydrogels, Anionic Polymerisation Nanocomposites SE - 2* **153,** 37–65 (Springer Berlin Heidelberg, 2000).

37. Mohan, N. & Nair, P. D. Polyvinyl Alcohol-Poly(caprolactone) Semi IPN Scaffold With Implication for Cartilage Tissue Engineering. *J Biomed Mater Res B Appl Biomater.* **84,** 584–594 (2008).

38. Hassan, C. M. & Peppas, N. A. Cellular PVA Hydrogels Produced by Freeze/Thawing. *J. Appl. Polym. Sci.* **76,** 2075–2079 (2000).

39. Campillo-Fernández, A. J. *et al.* Future design of a new keratoprosthesis. Physical and biological analysis of polymeric substrates for epithelial cell growth. *Biomacromolecules* **8,** 2429–36 (2007).

40. Pérez Olmedilla, M. *et al.* Response of human chondrocytes to a non-uniform distribution of hydrophilic domains on poly (ethyl acrylate-co-hydroxyethyl methacrylate) copolymers. *Biomaterials* **27,** 1003–12 (2006).

41. Soria, J. M. *et al.* Survival and differentiation of embryonic neural explants on different biomaterials. *J Biomed Mater Res A* **79,** 495–502 (2006).

42. Rico, P. *et al.* Substrate-induced assembly of fibronectin into networks: influence of surface chemistry and effect on osteoblast adhesion. *Tissue Eng. Part A* **15,** 3271–3281 (2009).

43. Gugutkov, D., Altankov, G., Rodríguez Hernández, J. C., Monleón Pradas, M. & Salmerón Sánchez, M. Fibronectin activity on substrates with controlled -OH density. *J. Biomed. Mater. Res. A* **92,** 322–31 (2010).

44. Salmerón Sánchez, M. *et al.* Role of material-driven fibronectin fibrillogenesis in cell differentiation. *Biomaterials* **32,** 2099–105 (2011).

45. Sancho-Tello, M. *et al.* Time evolution of ‘in vivo’ articular cartilage repair induced by bone marrow stimulation and scaffold implantation in rabbits. *Int. J. Artif. Organs.* (2015).

46. Diego, R. B., Estellés, J. M., Sanz, J., García-Aznar, J. M. & Salmerón Sánchez, M. Polymer Scaffolds With Interconnected Spherical Pores and Controlled Architecture for Tissue Engineering : Fabrication , Mechanical Properties , and Finite Element Modelin. *J Biomed Mater Res B Appl Biomater.* **81,** 448–455 (2007).

47. Diego, R. B., Gomez Ribelles, J. L. & Salmerón Sánchez, M. Pore collapse during the fabrication process of rubber-like polymer scaffolds. *J. Appl. Polym. Sci.* **104,** 1475–1481 (2007).

48. Chang, H. H., Yao, L.-C., Lin, D. & Cheng, L.-P. Preparation of microporous poly(VDF-co-HFP) membranes by template-leaching method. *Sep. Purif. Technol.* **72,** 156–166 (2010).

49. Vallés Lluch, A., Rodríguez-Hernández, J Gallego Ferrer, G. & Monleón Pradas, M. Synthesis and characterization of poly(EMA-co-HEA)/SiO2 nanohybrids. *Eur. Polym. J.* **46,** 1446–1455 (2010).

50. Vallés Lluch, A., Poveda-Reyes, S., Amorós, P., Beltrán, D. & Monleón Pradas, M. Hyaluronic acid-silica nanohybrid gels. *Biomacromolecules* **14,** 4217–4225 (2013).

51. Hassan, C. M. & Peppas, N. A. Structure and applications of Poly(vinyl alcohol) Hydrogels produced by conventional crosslinking or by freezing/thawing methods. *Adv. Polym. Sci.* **153,** 37–65 (2000).

52. Wong, B. L. & Sah, R. L. Effect of a focal articular defect on cartilage deformation during patello-femoral articulation. *J. Orthop. Res.* **28,** 1554–1561 (2010).

53. Guilak, F., Ratcliffe, A. & Mow, V. C. Chondrocyte deformation and local tissue strain in articular cartilage: A confocal microscopy study. *J. Orthop. Res.* **13,** 410–421 (1995).

54. Halonen, K. S. *et al.* Deformation of articular cartilage during static loading of a knee joint--experimental and finite element analysis. *J Biomech* **47,** 2467–2474 (2014).

55. Gibson, L. & Ashby, M. *Cellular solids: structure and properties*. (Cambridge University Press, 1997).

56. Gupta, S., Sinha, S. & Sinha, A. Composition dependent mechanical response of transparent poly(vinyl alcohol)

hydrogels. *Colloids Surfaces B Biointerfaces.* **78,** 115–119 (2010).

57. Hickey, A. S. & Peppas, N. A. Mesh size and diffusive characteristics of semicrystalline poly(vinyl alcohol) membranes prepared by freezing/thawing techniques. *J. Membr. Sci.* **107,** 229–237 (1995).

58. Vikingsson, L., Gomez-Tejedor, J. A., Gallego Ferrer, G. & Gomez Ribelles, J. L. An experimental fatigue study of a porous scaffold for the regeneration of articular cartilage. *J. Biomech.* (2015). doi:10.1016/j.jbiomech.2015.02.013

59. Vikingsson, L., Claessens, B., Gómez-Tejedor, J. A., Ferrer, G. G. & Gómez Ribelles, J. L. Relationship between micro-porosity, water permeability and mechanical behavior in scaffolds for cartilage engineering. *J. Mech. Behav. Biomed. Mater.* **48,** 60–69 (2015).

60. Lebourg, M., Suay Antón, J. & Gómez Ribelles, J. L. Porous membranes of PLLA–PCL blend for tissue engineering applications. *Eur. Polym. J.* **44,** 2207–2218 (2008).

61. Lebourg, M., Suay Antón, J. & Gómez Ribelles, J. L. Hybrid structure in PCL-HAp scaffold resulting from biomimetic apatite growth. *J Mater Sci Mater Med* **21,** 33–44 (2010).

62. Rodenas-Rochina, J., Gómez Ribelles, J. L. & Lebourg, M. Comparative study of PCL-HAp and PCL-bioglass composite scaffolds for bone tissue engineering. *J. Mater. Sci. Mater. Med.* **24,** 1293–1308 (2013).

63. Santamaría, V. A. *et al.* Influence of the macro and micro-porous structure on the mechanical behavior of poly (l-lactic acid) scaffolds. *J. Non. Cryst. Solids* **358,** 3141–3149 (2012).

64. Deplaine, H. *et al.* Biomimetic hydroxyapatite coating on pore walls improves osteointegration of poly(L-lactic acid) scaffolds. *J Biomed Mater Res B Appl Biomater* **101,** 173–186 (2013).

65. Martinez-Diaz, S. *et al.* In vivo evaluation of 3-dimensional polycaprolactone scaffolds for cartilage repair in rabbits. *Am J Sport. Med* **38,** 509–519 (2010).

66. Jurvelin, J. S., Buschmann, M. D. & Hunziker, E. B. Mechanical anisotropy of the human knee articular cartilage in compression. *Proc. Inst. Mech. Eng. H.* **217,** 215–219 (2003).